Computational Analysis of A Corrugated Dragonfly Airfoil At Low Reynolds Number

P Panneer Selvam, Assistant professor, Er.Perumal Manimekalai College of Engineering, Hosur, India. Selvam.aero311@gmail.com

R Jiniraj, Assistant professor, Er.Perumal Manimekalai College of Engineering, Hosur, India. jinirajaero@gmail.com

M Pughalendi, Assistant professor, Er.Perumal Manimekalai College of Engineering, Hosur, India. pugaz0635@gmail.com

Abstract: The chord Reynolds number of micro air vehicles are usually in the range of 10^4 to105. The laminar flow separation is a common phenomenon occurring in a flow over a body. The corrugated dragonfly airfoil has the potential ability to sustain an attached flow at low Reynolds number, thereby suppressing laminar flow separation or large laminar bubbles. In this project an optimized corrugated dragonfly airfoil is designed from the survey of standard airfoils. The flow properties of the corrugated dragonfly airfoil are measured at different angles of attack such as 0º, 5º, 10º and 15º for the Reynolds number of 5×10^4 in which the MAVs usually operates. The aerodynamic performance of corrugated dragonfly airfoil is compared with a traditional NACA 0012 airfoil at the same Re and also with a corrugated dragonfly airfoil at a different Re of 34000. The corrugated airfoil is meshed using GAMBIT and the computational fluid flow analysis is carried out using FLUENT on the corrugated dragonfly airfoil at low Reynolds number of 5×10^4. The flow behavior around the airfoil is analyzed and simulations are carried out to predict the behavior of unsteady flow structures around the airfoil at different angles of attack.

Keywords — Aerodynamics, Dragonfly, CFD, Reynolds Number.

I. INTRODUCTION

Micro-Air-Vehicles (MAVs), which typically refer to palm-sized aircraft (e.g. with a maximum dimension about 10cm and a flight speed about 10m/s), are of great interest to both military and civilian applications. Equipped with video cameras, transmitters or sensors, these miniaturized aerial vehicles can perform surveillance, reconnaissance, targeting, or bio-chemical sensing tasks at remote, hazardous or dangerous locations. A concerted effort supcported by the Defense Advanced Research Projects Agency (DARPA) in recent years has resulted in advancements in miniaturized digital electronics, micro fabrication, miniaturized power cells, remote communication, imaging and control devices and other enabling technologies. Such advances have turned the concept of MAVs as rapidly deployable eyes-in-the-sky from fiction into demonstrated facts. The continuing demand for such small and robust miniaturized aerial vehicles is making MAVs an emerging sector of the aerospace market, and MAVs are expected to become commonplace in the next ten to twenty years.

In this study, a simplified corrugated dragonfly airfoil is numerically analyzed in a steady free-stream flow. The aerodynamic performances are first compared to a traditional low Reynolds number airfoil: the NACA 0012.

Here the corrugated dragonfly airfoil is designed from the parameters obtained from the journals [1] and [3]. Computational fluid flow analysis should be carried out on the designed corrugated dragonfly airfoil to predict the improved aerodynamic performance parameters such as lift coefficient and drag coefficient compared with traditional airfoil NACA 0012.The earliest serious work on the development of airfoil sections began in the late 1800's [5]. Although it was known that flat plates would produce lift when set at an angle of incidence, some suspected that shapes with curvature that more closely resembled bird wings would produce more lift or do so more efficiently. H.F. Phillips patented a series of airfoil shapes in 1884 after testing them in one of the earliest wind tunnels in which states that artificial currents of air were produced from induction by a steam jet in a wooden trunk or conduit [7].

At nearly the same time Otto Lilienthal had similar ideas. After carefully measuring the shapes of bird wings, he tested the airfoil on a 7m diameter "whirling machine". Lilienthal believed that the key to successful flight was wing curvature or camber [8]. He also experimented with different nose radii

 DOI : 10.35291/2454-9150.2021.0061

and thickness distributions. Airfoils used by the Wright Brothers closely resembled Lilienthal's sections: thin and highly cambered. This was quite possibly because early tests of airfoil sections were done at extremely low Reynolds number, where such sections behave much better than thicker ones [10].

A number of hypotheses have been suggested to explain the fundamental mechanism of rather unexpected aerodynamic performance improvement of the corrugated dragonfly airfoils or wings over conventional smooth airfoils [12]. Newman, etc, al suggested that the improved aerodynamic performance would be associated with the earlier reattachment of the flow separation on the corrugated wings [15].

Most of the earlier experimental studies were conducted mainly based on the measurements of total aerodynamic forces (lift and drag) of either natural dragonfly wings or modeled corrugated wing sections [16]. More recently, Kesel has conducted pressure measurements on the surfaces of dragonfly wing model in addition to total lift and drag force measurements [18]. Kesel has found that negative pressure would be produced at the valleys of the corrugated dragonfly wing model, which would contribute to the increased lift. Vargas and Mittal [21] have conducted a numerical study of the flow around a 2D dragonfly model to investigate the flow behaviors around the corrugated dragonfly airfoil.

Dragonfly wings are not smooth or simple cambered surfaces. The cross-sectional camber of the wing has a well-defined corrugated configuration. [23] This design is of critical importance to the stability of this ultra-light construction given by Rees (1975a), Wootton (1992), Newman and Wootton (1986), Kesel et al. (1998). However, from an aerodynamic point of view, this cross section does not appear to be very suitable. The pronounced bends and edges should lead to high drag values. However, in visualizing experiments using profile models, Rees (1975b), Newman et al. (1977), and Rudolph (1978) and have shown that this geometry induces positive flow conditions. The vortices filling the profile valleys formed by these bends 'smooth down' the profile geometry as given by Kesel, 1998.

The aerodynamic characteristics of airfoils at a chord Reynolds number ($Re_C = \rho c U_\alpha/\mu$, where ρ and μ are the density and viscosity of the fluid, respectively, U_α is the free-stream velocity and c is the chord length of an airfoil) of less than 5×10^5 are becoming increasingly important from both fundamental and industrial point of view, due to recent developments in small wind turbines, small unmanned aerial vehicles (UAVs), micro-air vehicles (MAVs), as well as researches on bird/insect flying aerodynamics (Lin and Pauley, 1996). For example, at the starting stage of a 500W wind turbine, the tip Rec increases from 1×10^4 to 1×10^5, and the angle (α) of attack reduces gradually from 86º to 20º. A similar variation in α occurs during insect flight, but Re_C may be even lower as in Wang, 2005. For UAVs and MAVs, Re_C is commonly in the range of 1×10^5 to 6×10^5. However, such low Re_C problems have not been addressed sufficiently in the literature, let alone when combined with large angle of attack. General researches on airfoil aerodynamics have focused on conventional aircraft design with Re_C beyond 5×10^5 and α below stall.

The aerodynamics of hovering insect flight was explored by Ellington (1984). Usherhood and Ellington (2002) investigated forces acting on hawkmoth and bumblebee wings in 'propeller- like' revolution at $Re_C = 1.1\times10^3$ to 2.6×10^4. The steadily revolving wings produced high lift and drag, which was described to the formation of a leading-edge vortex. Miklosovic et al. (2004) measured in a wind tunnel the lift and drag on a flipper of a humpback whale ($Re_C = 5.05\times10^5$ to 5.2×10^5). They observed that the stall angle of a flipper with a leading edge protuberance could be enlarged by approximately 40%, relatively to a flipper with a smooth leading edge, which led to increased lift and decreased drag.

II. CORRUGARED DRAGONFLY AIRFOIL

Early wind tunnel experiments on scale-pleated models of insect wings conducted by Rees (1975b) on Aerodynamic properties of an insect wing section and a smooth aerofoil compared, and Rudolph (1977) on Aerodynamic properties of Libellula quadrimaculata and the flow around smooth and corrugated wing section models during gliding flight suggested that the pleated configuration has no aerodynamic significance. Rees (1975b) and Rudolph (1977) both concluded that fluid flowing over the pleated airfoil becomes trapped between the folds where it either becomes stagnant or rotates slowly, resulting in the pleated airfoil functioning as a streamlined airfoil. The only advantage of the pleated airfoil over the technical airfoils as noted by Rudolph (1977) was that it delayed flow separation at higher angles of attack, and a stall did not occur abruptly.

Okamoto. M and Azuma. A (1996) conducted several detailed experiments to investigate the aerodynamic characteristics of dragonfly wings and model wings at a Reynolds number ranging from 11,000 to 15,000. Their experiments consisted of force and moment measurements in a horizontal wind tunnel, auto-rotational flights in a vertical wind tunnel and gliding flight in still air. The effects of thickness, camber, pleats and leading edge sharpness were all tested using various models to examine the lift curve slope, maximum lift coefficient, and minimum drag coefficient and lift-to-drag ratio. From their experiments, a thinner flat plate with camber and a sharp leading edge is the profile that provides the best lift at these low Reynolds numbers. The tests also indicated that the pleated plate outperformed the flat plate at all angles of attack. The orientation of the

 DOI : 10.35291/2454-9150.2021.0061

leading edge of the pleated plate had a significant effect on the lift generated at high angles of attack. They concluded that a downward facing leading edge had a much better performance than an upward facing leading edge. Experimental tests on actual dragonfly wings from an Anax parthenope julius produced a $C_{L,max}$ of 1.05, which was higher than that produced by streamlined airfoils.

Wakeling and Ellington (1997) also come to the same conclusion from their paper Dragonfly flight: I, Gliding flight and steady-state aerodynamic forces, when filming free gliding dragonflies and conducting wind tunnel experiments on their wings at a Reynolds number ranging from 700 to 2400. $C_{L,max}$ recorded for free gliding dragonflies was 0.93 and 1.07 when tested in a wind tunnel environment. Wakeling and Ellington (1997) stated that the enhanced lift produced by dragonflies is not attributed to the Reynolds number, the aspect ratio or the wing area, but rather a surface feature, mainly the corrugations found in dragonflies.

Antonio B. Kesel(2000) compared the aerodynamic characteristics of dragonfly wing sections with technical airfoils. He suggested that during gliding, dragonfly wings can be interpreted as acting as ultra-light airfoils which, for static reasons, have a well-defined cross-sectional corrugation. This corrugation forms profile valleys in which rotating vortices develop. The cross-sectional configuration varies greatly along the longitudinal axis of the wing. This produces different local aerodynamic characteristics. He analyze the C_L/C_D characteristics using a force balance system at Reynolds number of 7880 and 10000 and found that all cross sectional corrugation geometries have very low drag coefficients closely resembling those of flat plates but attain much higher lift values than flat plates. The orientation of the leading edge does not play an important role. The detectable lift forces can be compared with those of technical wing profiles for low Re numbers. From the pressure measurement results, he revealed that because of rotating vortices along the chord length, not only is the effective profile form changed, but the pressure relationship on the profile is also changed. Irrespective of the side of the profile, negative pressure is produced in the profile valleys and net negative pressure on the upper side of the profile is reached only at angles of attack greater than 0º. These results demonstrate the importance of careful geometrical synchronization as an answer to the static and aerodynamic demands placed upon the ultra-light airfoils of a dragonfly.

Kesel (2000) extracted three cross-sections at different positions along the span of a wing of an Aeschna cyanea to develop the pleated models. The aerodynamic performance of the pleated models was compared to its corresponding profiled airfoil at a chord Reynolds number of 10000, and the results showed that the pleated airfoils generated higher lift than the profiled airfoils. Pressure measurements performed on a model that represented the front portion of a pleated airfoil showed that a net negative pressure sufficient to produce lift occurred only at angles of attack greater than 0◦.

The journal experimental investigations on biologically inspired airfoils for MAV applications by Masatoshi Tamai in 2007 explore the possibilities of corrugated dragonfly airfoil as MAVs applications. They conducted two experimental studies to explore the possibilities of biologically inspired airfoils as Micro-Air-Vehicles (MAVs) applications. In the first study, the flow behavior around a corrugated dragonfly airfoil compared with both a traditional streamlined airfoil and a flat plate were investigated.

Masatoshi Tamai and Hui Hu in 2008 conducted an experimental study of flexible membrane airfoils at low Reynolds number to explore its benefits for MAV applications. In addition to measuring aerodynamic forces acting on the flexible membrane airfoils/wings, a high-resolution Particle Image Velocimetry (PIV) system was used to conduct flow field measurements to quantify the transient behavior of vortex and turbulent flow structures around the flexible membrane airfoils/wings at different angles of attack. The force measurement results revealed that flexible membrane airfoils can provide better aerodynamic performance compared with their rigid counterpart at low Reynolds numbers. The velocity of the incoming flow was set as U_α= 11 m/s, which corresponds to a chord Reynolds number of Re_c = 70,000. The turbulence intensity of the incoming flow was found to be about 0.8%, measured by using a hotwire anemometer. The flexible membrane airfoils FM02, FM03 and FM10 were found to have very comparable or slightly larger lift coefficient compared with the rigid thin airfoil.

Shi Sheng-Xian and Chen Jian-min in 2012 conducted an experimental study of flow around a bio-inspired airfoil at Reynolds number 2×10^3 by measuring the fluid flow around a bio-inspired airfoil with corrugated surfaces and its smooth counterpart at different angles of attack (0º, 4º, 8º, and 12 º) by using Particle Image Velocimetry (PIV). They concluded that due to the fact that dragonfly wing is practically flexible, it is speculated that the wing structure of a gliding dragonfly might be sophisticatedly deformed in response to the periodic loading to reduce the drag**.**

III. METHODOLOGY

Computing unsteady flows at low to moderate Reynolds numbers continues to be of serious interest thanks to its application in MAVs and its relevance to insect and bird flights. Flapped flight of bird is the better example of optimum motion of aerodynamic surfaces that the same time it develops necessary thrust for forward motion and creates lift to keep it airborne. It is now accepted that theoretical studies involving steady-state aerodynamics is of limited

 DOI : 10.35291/2454-9150.2021.0061

value and a few unsteady flow models are studied. For example, a flapping wing inviscid flow model has been proposed and it provides an extensive review of early aerodynamic models of flapping flight. However, it is essential that any unsteady flow model must include viscous effects involving separation and transition in the presence of large vortices. This has been attempted by using CFD techniques to study flapping flight, where the airfoil executes heaving oscillations being placed in a uniform flow. In commercial software, based on finite volume primitive variable formulation is used to solve Navier- Stokes equation in Lagrangian- Eulerian framework. In three-dimensional incompressible Navier-Stokes equation, the primitive variables have been solved in strong conservation form using SIMPLEC and PISO methods. Sun & Tang have reported solving three- dimensional Navier-Stokes equation using the artificial compressibility method. Spatial discretization was performed by third order upwind flux-difference splitting and time integration by second order Adams-Bashforth technique. Relatively good agreement was reported with experimental data.

This time strategy of integration displays computational with large error for unsteady flows. Gustafson & Leben have used this formulation to compute hovering flight of an elliptic cylinder. Unfortunately, the governing VTE written in the moving frame had an important angular acceleration term omitted erroneously. For the flapping motion, vortex shedding was investigated and an optimal flapping frequency based on time scales associated with shedding of leading and trailing edge vortices is reported. In solving this issue a second-order finite difference scheme, the Navier- Stokes equation is solved for an airfoil.

3.1. Solver settings

The equations are integrated in time using the fractional step method (Abel Vargas 2008). In this method, a modified N-S equation is solved and an intermediate velocity is obtained by staggered grid.

$$\frac{\partial}{\partial t}(\rho u_i) + \frac{\partial}{\partial x_j}\left[\rho u_i u_j + p\delta_{ij} - \tau_{ji}\right] = 0, \quad i = 1,2,3$$

$$\frac{\partial}{\partial t}(\rho e_0) + \frac{\partial}{\partial x_j}\left[\rho u_j e_0 + u_j p + q_j - u_i \tau_{ij}\right] = 0$$

A second order upwind differentiation scheme is implemented for the convective terms, while the diffusion terms are discretized with an implicit Crank–Nicolson technique which as a truncation error constraint. The solver uses the below conditions for solving the process. Pressure-based, steady, 2D equations are used since the process is mainly based on the pressure related. SST k-ω turbulence model is used to predict the vortex structures formed near the corrugations which in turn results in an attached flow.

$$\frac{\partial}{\partial t}(\rho k) + \frac{\partial}{\partial x_i}(\rho k u_i) = \frac{\partial}{\partial x_j}\left[\left(\mu + \frac{\mu_t}{\sigma_k}\right)\frac{\partial k}{\partial x_j}\right] + P_k + P_b - \rho\epsilon - Y_M + S_k$$

$$\frac{\partial}{\partial t}(\rho\epsilon) + \frac{\partial}{\partial x_i}(\rho\epsilon u_i) = \frac{\partial}{\partial x_j}\left[\left(\mu + \frac{\mu_t}{\sigma_\epsilon}\right)\frac{\partial \epsilon}{\partial x_j}\right] + C_{1\epsilon}\frac{\epsilon}{k}(P_k + C_{3\epsilon}P_b) - C_{2\epsilon}\rho\frac{\epsilon^2}{k} + S_\epsilon$$

The second step of the fractional step method is the solution of a pressure correction equation by solving a Poisson equation. The Poisson equation, being the most time consuming part of the solution algorithm, is solved with a flexible and efficient geometric multi-grid algorithm with a flexible semi-coarsening strategy which employs a Gauss–Siedel line-SOR (Successive over Relaxation) smoother. The factors considered during this study are the flapping frequency, the inclined angle of stroke plane and therefore the stroke amplitude. The unsteady lift/thrust forces are obtained by solving the unsteady laminar Navier-Stokes equations with the conformal hybrid mesh.

$$\overline{\Phi} \equiv \frac{1}{T}\int_T \Phi(t)dt$$

$$\Phi' \equiv \Phi - \overline{\Phi}$$

The governing equations are the time dependent incompressible Reynolds-averaged Navier-Stoke's equations including of continuity equation and momentum equation as The non-dimensional form of the Navier–Stokes equations is discretized using a cell-centered, collocated (non-staggered) arrangement where all variables (i.e. velocity components and pressure) are located at an equivalent physical location. Staggered, unsteady pressure- based solver is chosen because of the flow field is assumed as incompressible unsteady flow.

$$\tau_{ij} = 2\,\mu_t\,S^*_{ij} - \frac{2}{3}k\delta_{ij}$$

Still there is a need to specify a turbulence length scale, which is also a flow dependent property. Hence one still needs to have certain knowledge about the studied flow in advance. Therefore such models are called incomplete. Both zero- and one-equation models are incomplete.

$$-\rho\overline{u_i' u_j'} = \mu_t\left(\frac{\partial u_i}{\partial x_j} + \frac{\partial u_j}{\partial x_i} - \frac{2}{3}\frac{\partial u_k}{\partial x_k}\delta_{ij}\right) - \frac{2}{3}k\delta_{ij}$$

3.2. Proposed Method

The chord Reynolds number of micro air vehicles are usually in the range of 104 to 105. The laminar flow separation is a common phenomenon occurring in a flow over a body. In this study an optimized corrugated dragonfly airfoil is designed from the survey of standard airfoils. Airfoil is to be

 DOI : 10.35291/2454-9150.2021.0061

designed using GAMBIT software. A computational fluid flow analysis is to be carried out on the corrugated dragonfly airfoil at low Reynolds number where MAVs usually operates to analyze the flow behavior around the airfoil. The working fluid is air and the flow field is assumed to be incompressible and laminar with constant thermo physical properties. The results are compared with a NACA 0012 airfoil of same Reynolds number and corrugated dragonfly airfoil of different Reynolds number.

3.3. *Airfoil and domain modelling*

The process of airfoil design proceeds from a knowledge of the boundary layer properties and the relation between geometry and pressure distribution. In these cases, airfoils may be chosen from catalogs such as Selig's Airfoils at Low Speeds. The advantage to this approach is that there is test data available. Compared with standard NACA airfoils, the GA (W)-1 airfoil was specially designed for low-speed aviation applications with a large leading-edge radius to flatten the peak in the pressure-coefficient profile near the airfoil nose to discourage flow separation. The GA (W)-1 airfoil has a maximum thickness of 17% of the chord length. The flat plate has a rectangular cross section. Based on the expressions for laminar separation, one finds that an all-laminar section can generate a C_L of about 0.4 or achieve a thickness of about 7.5%.

The corrugated dragonfly airfoil is designed using GAMBIT software. The constraints for designing the airfoil are taken from the journal Computational Study of Unsteady Flows around Dragonfly and Smooth Airfoils at Low Reynolds Numbers by H. Gao, Hui Hu, Z. J. Wang. The dimensions are shown in the below figure.

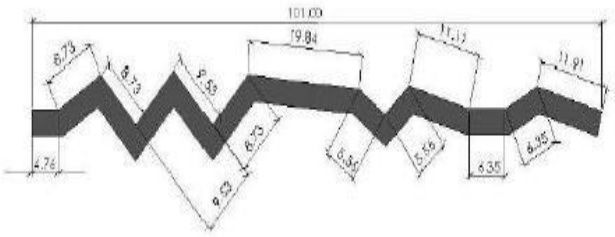

Fig.3.1. Dimensions of Corrugated Dragonfly Airfoil

The maximum effective thickness of the corrugated airfoil (i.e., the airfoil shape formed by fitting a spline through the protruding corners of the corrugated cross section) is about 15% of the chord length, which is slightly smaller than that of the streamlined GA(W)-1 airfoil (17% of the chord length). The bioinspired corrugated airfoil has the chord length of C=100 cm.

Grid generation is done with the help of gambit software. The grid must then be transformed from the physical domain into a computational domain, which is a form that the flow solver program understands and uses to perform the numerical calculations described below. The domain is 12 times the chord length from the corrugated dragonfly airfoil.

The grid for the corrugated dragonfly aerofoil model was generated using the GAMBIT software. Structured grid was used for the 2D analysis of the model with quadrilateral cells. The CH-grid scheme with quad type cells of volume meshing in GAMBIT was used to make the grid. Initially coarser grids with approximately 17540 cells were made for the inviscid calculation. The grid consists of 16180 nodes and 17540 quadrilateral cells.

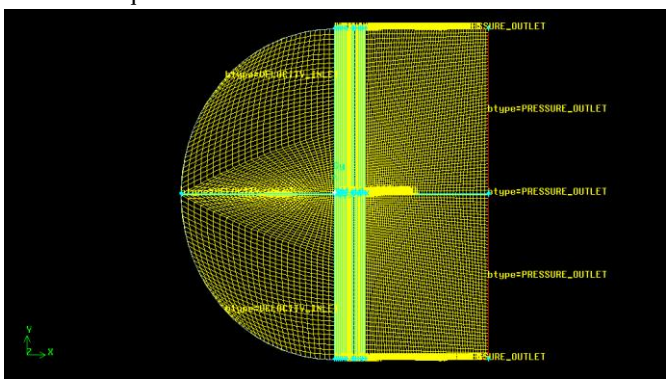

Fig.3.3. Grid System for Corrugated Dragonfly Airfoil

Velocity inlet boundary condition was set to the inlet face (i.e., face C of the CH domain), where the velocity at which the flow passes the aerofoil is specified. Pressure outlet boundary condition was set to the outlet face (i.e., vertical length of the face H in the CH domain), where the variables are to be extrapolated from the interior cells. The upper and lower surface of the corrugated dragonfly aerofoil was assigned as wall boundary condition.

The meshed corrugated aerofoil along with the given boundary conditions is solved using the FLUENT software. Inlet velocity is set for AOA 0°, 5°, 10° and 15°. The operating pressure is set as atmospheric pressure. The boundary condition is given as that the inlet velocity is 7.3 m/s at a Reynolds number of 5×10^4.

IV. PERFORMANCE ANALYSIS

The results obtained from the computational tests revealed the increased performance of the corrugated dragonfly aerofoil at Re of 5×104 over the other which are compared. The dynamic pressure variation contour is explained in graphically in fig (a), (b), (c) and (d).

From all these contour diagram of dynamic pressures at different angles of attack, it is clear that the pressure difference between the upper and the lower surface is greater at 15 degrees of angle of attack. The greater the pressure difference, the greater the lift since every object moves from higher pressure to lower pressure. Therefore maximum lift can be obtained at this angle of attack.

 DOI : 10.35291/2454-9150.2021.0061

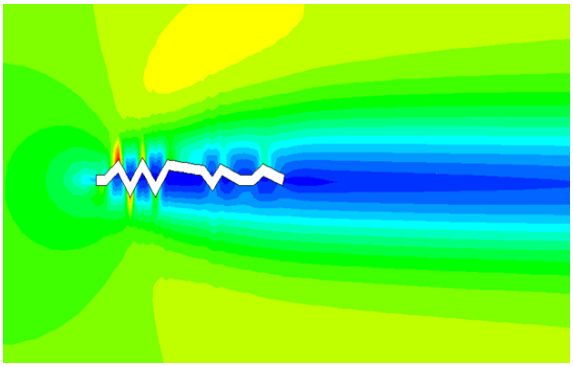

Fig.4.1.(a) Dynamic pressure at 0^0 AOA

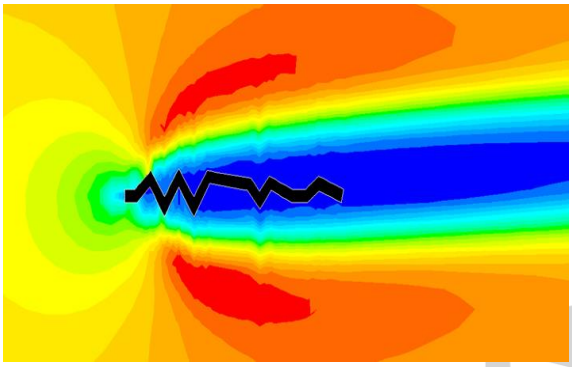

Fig. 4.1.(b) Dynamic pressure at 5^0 AOA

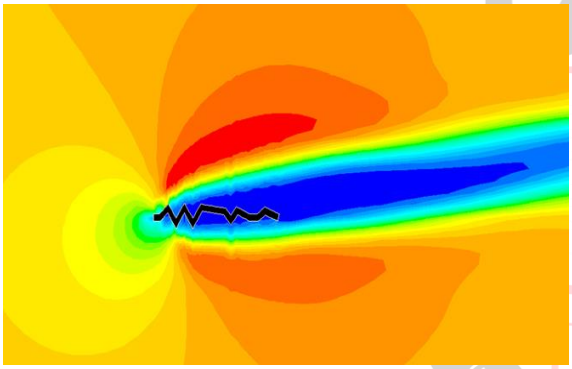

Fig. 4.1(c) Dynamic pressure at 10^0 AOA

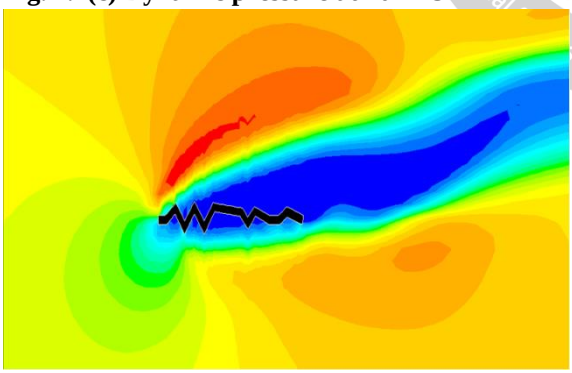

Fig. 4.1(d) Dynamic pressure at 15^0 AOA

The velocity contours shows the variation of velocity along the surface of the corrugated dragonfly aerofoil. At 0 degree angle of attack, the velocity distribution of air on both sides of the aerofoil is found to be the same. The variation of velocity distribution increases as the angle of attack increases. At 15 degree angle of attack, the velocity distribution on the upper aerofoil surface is seen to be more varied from the lower surface. It can be understood from the velocity magnitude contour diagram shown below.

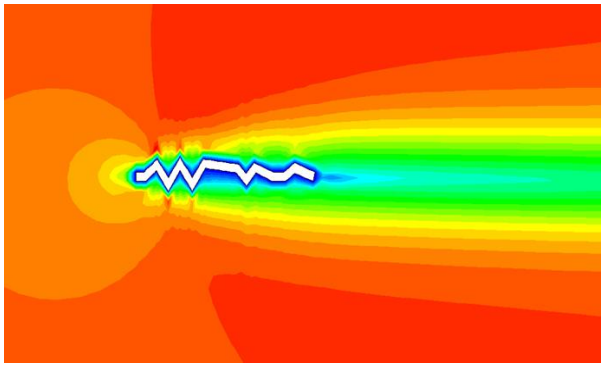

Fig.4.2.(a) velocity contour at 0^0 AOA

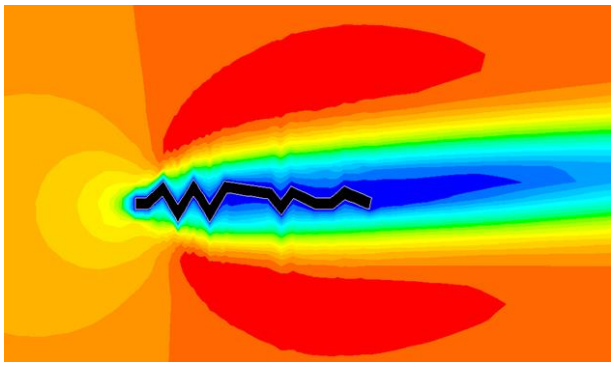

Fig. 4.2.(b) velocity contour at 5^0 AOA

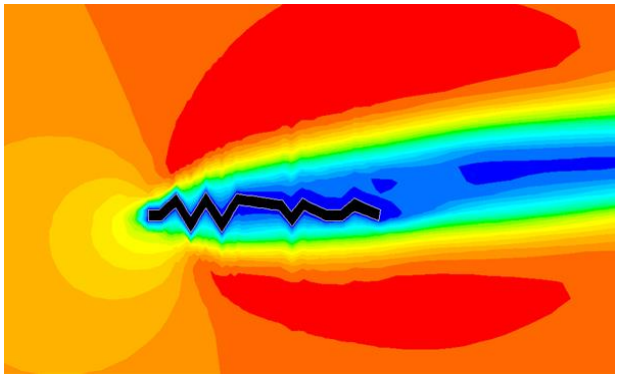

Fig. 4.2(c) velocity contour at 10^0 AOA

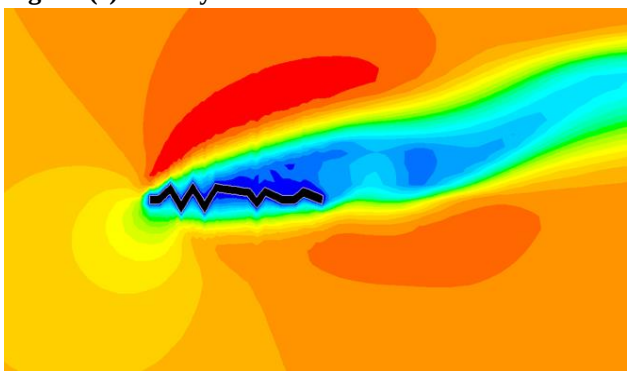

Fig. 4.2 (d) velocity contour at 15^0 AOA

The direction of flow over the corrugated dragonfly aerofoil is shown in the velocity vector contour. At 0º angle of attack, the flow direction is same at all the points. As the angle of attack increases from 5º to 15º, the reversed flow is formed on the upper surface of the aerofoil. The contours of velocity vector at different angle of attack are shown below.

 DOI : 10.35291/2454-9150.2021.0061

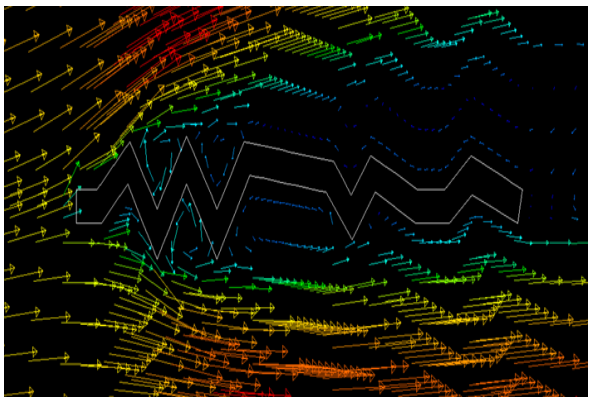

Fig.4.3.(a) velocity vector at 5^0 AOA

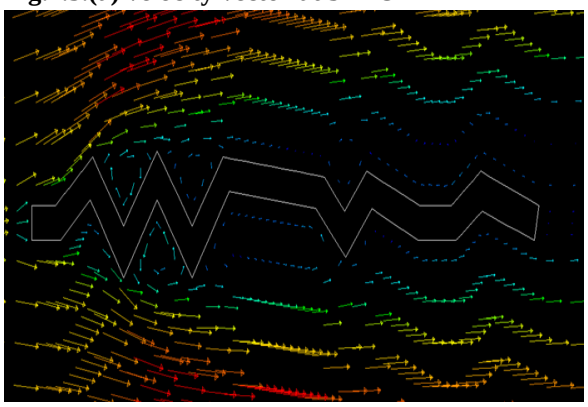

Fig. 5.1.(b) velocity vector at 10^0 AOA

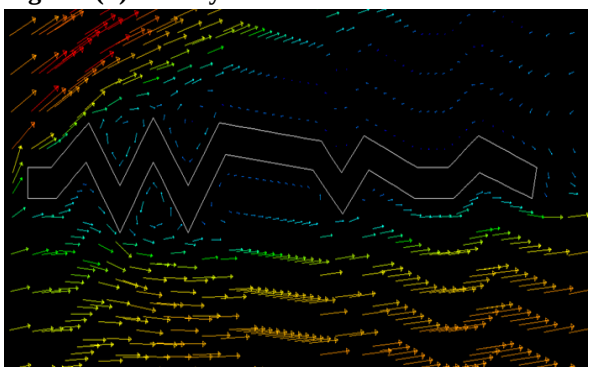

Fig.4.3.(c) velocity vector at 15^0 AOA

These velocity vector contours clearly shows the direction of flow over the corrugated dragonfly aerofoil at different angles of attack. The co-efficient of pressure (C_P) is plotted for different angle of attack along the chord length. At large angle of attack, the co-efficient of pressure between the upper and lower aerofoil surface is greater and it increases till the stalling angle. The co- efficient of pressure plots for different angle of attack is shown below.

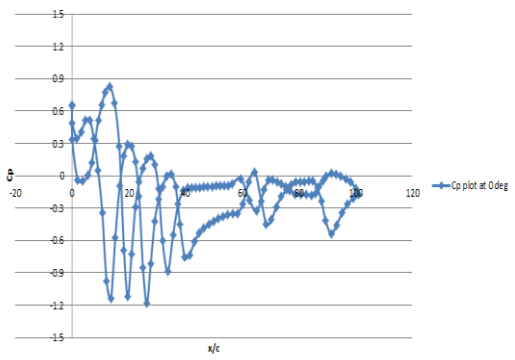

Fig.4.4 Co-efficient of pressure vs x/c plot at 0º AOA

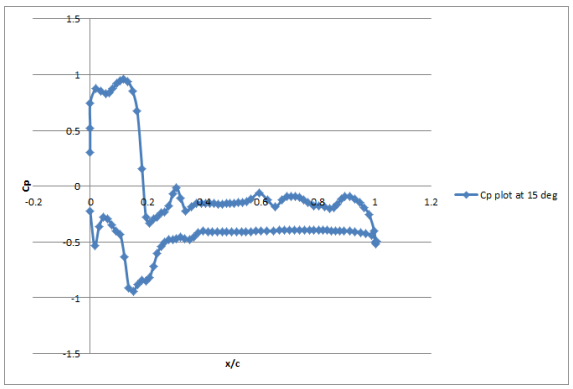

Fig.4.5 Co-efficient of pressure vs x/c plot at 5º AOA

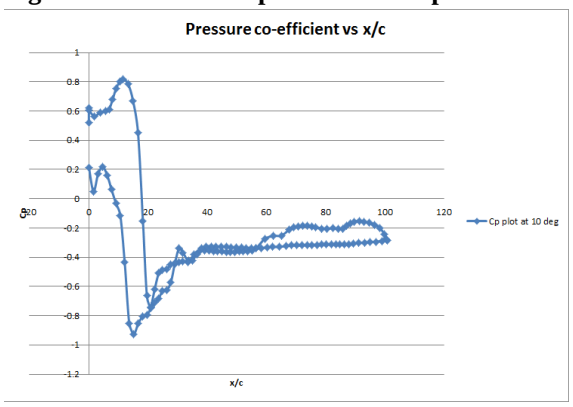

Fig.4.6 Co-efficient of pressure vs x/c plot at 10º AOA

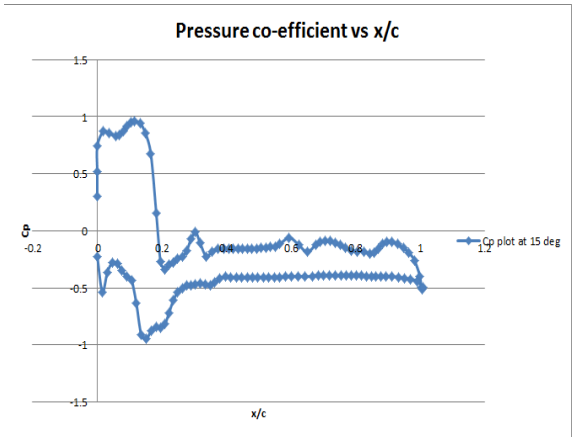

Fig.4.7 Co-efficient of pressure vs x/c plot at 15º AOA

From these C_P plots, it is found that increasing the angle of attack increases the difference in pressure co-efficient between the upper and lower aerofoil surface. At 15º angle of attack, the pressure co-efficient difference is more resulting in high lift co-efficient. The flow separation point is found out for the entire angle of attack 5 º, 10º and 15º from the velocity vector plot. The line/rake is selected and a line on the aerofoil surface is created at the point where the reversed flow occurred, using the line tool option. The velocity along the x-direction is found out and the point at which the flow reverses is the flow separation point. The flow separation points for the different angle of attack are plotted as shown below.

 DOI : 10.35291/2454-9150.2021.0061

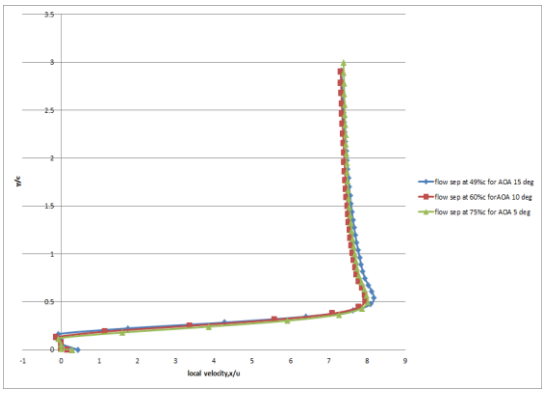

Fig.4.8 X-Velocity Vs Y/C Plot

The flow separation point for different angle of attack is found out from the velocity vector diagram. At 0º angle of attack, flow is not separated. At 5º angle of attack, flow separation occurs at 75% of chord. At 10º angle of attack, flow separation occurs at 60% of chord. At 15º angle of attack, flow separation occurs at 49% of chord. It is found that the flow separation point is delayed in corrugated dragonfly aerofoil compared to traditional streamlined NACA 0012 aerofoil. The flow separation point measured in the velocity vector plot is shown clearly in the below figure. The aerodynamic performance such as lift co-efficient of the corrugated dragonfly aerofoil is compared with that of the NACA 0012 aerofoil at same Reynolds number. Also the lift co-efficient of corrugated dragonfly aerofoil at a Reynolds number of 34000 is taken from the base paper and is compared with the analysed corrugated dragonfly aerofoil at Reynolds number of 5×10^4.

The lift co-efficient values of NACA 0012 aerofoil for different angle of attack such as 0º, 5º, 10º and 15º obtained from the base paper are 0,0.387, 0.802 and 0.905 respectively at Reynolds Number was 5000. Similarly The lift co-efficient values of Corrugated Dragonfly Aerofoil at Re=34000 for different angle of attack such as 0º, 5º, 10º and 15º are 0.12, 0.543 1.082 and 1.245 respectively.

The lift co-efficient values of corrugated dragonfly aerofoil at a Reynolds number of 5×10^4 for different angle of attack such as 0º, 5º, 10º and 15º measured from the analysis results of FLUENT are0.15, 0.587, 1.125 and 1.296 respectively. The lift co-efficient result reveals that the corrugated dragonfly aerofoil at Reynolds number 5×10^4 has the highest performance compared to the other two. Thus corrugated dragonfly aerofoil can be highly used in micro air vehicles working at a low Reynolds number of 5×10^4 than the traditional streamlined aerofoil.

The below figure shows the comparison of the lift co-efficient for different angle of attacks for the corrugated dragonfly aerofoil and the traditional streamlined NACA 0012 aerofoil at same low Reynolds number of 50000. From this lift co- efficient plot, it is understood that corrugated dragonfly aerofoil is suitable for the low speed micro air vehicle applications. This improved aerodynamic performance of corrugated dragonfly aerofoil is due to the presence of corrugations which sustains an attached flow at low Reynolds number. The effect of vortices formation does not affect the aerodynamic performance at low speeds.

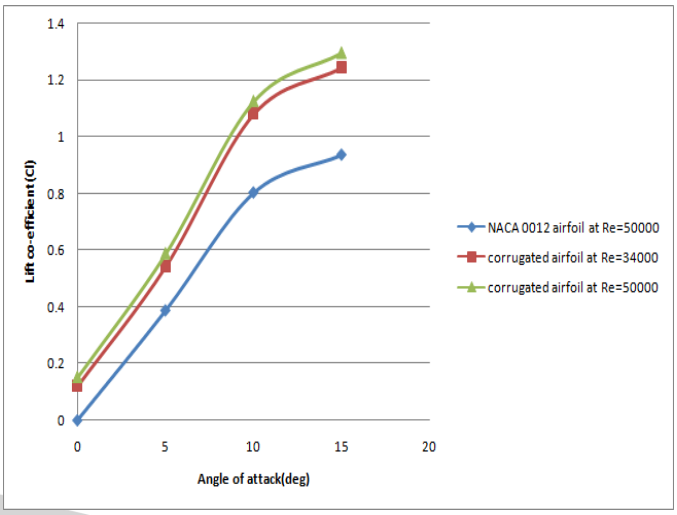

Fig.4.9 Lift Co-Efficient Vs Angle Of Attack Plot

V. CONCLUSION

The corrugated dragonfly aerofoil is analysed at low Reynolds number of 50000 and the flow properties are obtained. The flow separation point is found out which is suppressed than that occurs in conventional streamlined aerofoil. Suppression of the flow separation point results in delaying of stall angle. The lift co-efficient measurement result shows the improved aerodynamic performance of the corrugated dragonfly aerofoil compared to that of traditional NACA 0012 aerofoil. This increased C_L is due to the suppression of flow separation point caused due to the presence of corrugations. Therefore more lift is occurred for corrugated dragonfly aerofoil than for streamlined aerofoil at same angle of attack. Also the corrugated dragonfly aerofoil at Reynolds number of 34000 is compared in this study and the improvement of lift co-efficient is noted.

REFERENCES

[1] Alain Pelletier and Thomas J. Mueller, *''Low Reynolds Number Aerodynamics of Low-Aspect-Ratio, Thin/Flat/Cambered-Plate Wings''*, University of Notre Dame, Notre Dame, Indiana 46556, JOURNAL OF AIRCRAFT, Vol. 37, No. 5, September–October 2000.

[2] Alain Pelletier, *"A Study of the Nonlinear Aerodynamic Characteristics of a Slender Double-Delta Wing in Roll."* Ph.D. Dissertation, The University of Notre Dame, April 1998.

[3] Alexander D E 1984, *''Unusual phase relationships between the forewing and hindwings in flying dragonflies''*, J. Exp. Biol. 109.

 DOI : 10.35291/2454-9150.2021.0061

[4] Azuma A 1992, "*The Biokinetics of Flying and Swimming (Berlin:Springer)".*

[5] Azuma A and Watanabe T 1988, *''Flight performance of a dragonfly''* J. Exp. Biol. 137.

[6] Brodsky A K 1994, *''The aerodynamics of insect flight The Evolution of Insect Flight''*, New York, Oxford University Press.

[7] Buckholz R H 1986, *"The functional role of wing corrugations in living systems",* J. Fluids Eng. 108.

[8] Carmichael, B. H. *"Low Reynolds Number Airfoil Survey."* Volume I, NASA Contractor Report 165803, November 1981. DOI: 10.1016/S1001- 6058(11)60262-X.

[9] Ellington C P 1984a, *"The aerodynamic of hovering insect flight: I",* The quasi-steady analysis Phil. Trans. R. Soc. 305.

[10] Ennos A R 1989, *''The effect on the optimal shapes of gliding insect and seeds''*, J. Zool. 219.

[11] Hankin M A 1921, *''The soaring flight of dragonflies''*, Proc. Camp. Phil. Soc. 20.

[12] Jane Z, Wang, *''Dissecting insect flight''*. Annu Rev Fluid Mech 2005.

[13] Kesel, Antonia B. *"Aerodynamic characteristics of dragonfly wing sections compared with technical aerofoils".* J Experiment Biol 2000.

[14] KWOK R., MITTAL R. *, "Experimental investigation of the aerodynamics of a modeled dragonfly wing section[C]".* AIAA region I-MA student conference. Charlottesville, Virginia, 2005.

[15] Laitone, E. V. *"Aerodynamic Lift at Reynolds Numbers below 7×10^4",* AIAA Journal, Vol. 34, No. 9, September 1996.

[16] Lissaman, P. B. S., 1983, *"Low-Reynolds-Number Airfoils*," Annual Review of Fluid Mechanics, Vol. 15.

[17] Miley, S. J. *"An Analysis of the Design of Airfoil Sections for Low Reynolds Numbers",* Ph.D. Dissertation, Mississippi State University, 1972.

[18] Newman D J S and Wootton R J 1986, *" An approach to the mechanics of pleating in dragonfly wings"*. J. Exp. Biol.

[19] Newman, B. G., Savage, S. B., and Schouella, D., *"Model Test on a Wing Section of an Aeschna Dragonfly,"* Scale Effects in Animal Locomotion, edited by T. J. Pedley, Academic Press, London, 1977.

[20] Okamoto M, Yasuda K and Azuma A 1996, *''Aerodynamic characteristics of the wings and body of a dragonfly"*, J. Exp. Biol. 199.

[21] Rees C J C 1975b , *"Aerodynamic properties of an insect wing section and a smooth aerofoil compared",* Nature.

[22] Rudolph R 1977, " *Aerodynamic properties of Libellula quadrimaculata L. (Anisoptera: Libelludidea), and the flow around smooth and corrugated wing section models during gliding flight",* Odonatologica.

[23] Rüppel, G. (1989), *''Kinematic analysis of symmetrical flight manoeuvres of Odonata''*, J. Exp. Biol. 144.Savage S B, Newman B G and Wong D T M 1979, *''The role of vortices and unsteady effects during the hovering flight of dragonflies''*, J. Exp. Biol. 83.

[24] SHI Sheng-xian, LIU Ying-zheng, CHEN Jian-min, *''An Experimental Study Of Flow Around A Bio-Inspired Airfoil At Reynolds Number 2.0×10^3''*, Shanghai Jiao Tong University, Shanghai 200240, Journal of hydrodynamics, 2012,24(3):410-419

[25] Somps C and Luttges M 1985, *''Dragonfly flight: novel uses of unsteady separated flow'',* Science 228.

[26] Tamai M, Zhijian Wang, Ganesh Rajagopalan, Hui Hu, 2007, *''Aerodynamic Performance of a Corrugated Dragonfly Airfoil Compared with Smooth Airfoils at Low Reynolds Numbers'',* In 45th AIAA Aerospace Sciences Meeting and Exhibit, Reno, Nevada, Jan.

[27] Tamai, M., *"Experimental investigations on biologically inspired airfoils for MAV applications",* Master thesis, Aerospace Engineering Department, Iowa State University, Nov., 2007.

 DOI : 10.35291/2454-9150.2021.0061